UPPSALA
UNIVERSITET

Impact of Viral Geometry and Cellular Lipid Environment on Virus-Endosome Fusion Kinetics

Valeria Aguilar Quiñones

Master Degree Project in Infection Biology, 120 credits. Spring 2021
Department: Institute of Cell and Molecular Biology
Supervisor: Peter Kasson
Co-supervisor: Ana Villamil Giraldo

Table of contents

Abstract

The great majority of emerging or re-emerging diseases are caused by enveloped viruses such as hantaviruses, Nipah virus or Ebola virus. All diseases threatening public health categorized by the World Health Organization (WHO) as needed for urgent research and development for their epidemic potential or lack of countermeasures are caused by enveloped viruses. Some of these diseases are COVID-19, Crimean-Congo haemorrhagic fever or Zika[1].

Characterizing membrane fusion and understanding the kinetics of the process will help us gain knowledge on how enveloped viruses infect cells. Such knowledge can be used for therapeutic purposes and in therapy strategy design (e.g., drug design). In this project we aimed to address the role of viral morphology in the fusion process. A pleomorphic virus, like influenza A virus, was chosen to study fusion kinetics in filamentous and spherical viral particles using fluorescence dequenching assays. Fusion events were monitored by lipid mixing in microfluidic flow cells using liposomes and were determined by measuring changes in fluorescence of labelled viruses. However, fusion kinetics could only be determined with the spherical virions. The main reasons for this are discussed in the report. The low concentration of the filamentous virus was probably the major cause, which implies a further optimization of the sample prior lipid mixing monitoring in viruses with a low titre using this experimental system. This could be achieved by viral propagation in tissue cultures.

Popular summary

Viruses that have an outer lipidic membrane are known as enveloped viruses. These types of viruses, such as HIV, dengue virus (DENV), influenza virus, or coronaviruses, which cause severe diseases that affect the human population, share one step in their infectious cycle – membrane fusion. It is a crucial step which enables the viruses either to enter the target cell or once inside, escape from the cellular compartment in which they reside (endosomes) and release their genetic content so that it can interact with the cell machinery and more viral particles are produced. The fusion process consists, basically, in making one single lipidic membrane out of two and it is mainly driven by viral proteins, e.g., haemagglutinin (HA) from influenza A virus (IAV). Taking influenza viruses as an example, fusion is triggered by acidification of the endosomes. The viruses that are enclosed within endosomes are exposed to a low pH (~ 5) that leads to structural changes in the HA protein exposing the fusion peptide which is inserted into the target membrane. Both membranes will be pulled together and eventually a pore would be formed finalizing the process.

In this project, we wanted to address the impact of viral morphology, i.e., the shape adopted by viral particles, on how fast the membrane fusion process occurs, which is defined as fusion kinetics. Thus, two different strains from IAV belonging to a same subtype (H3N2) were chosen to study their fusion kinetics. An influenza strain that forms predominantly filamentous viral particles (Udorn) and another one that is mainly spherical (X-31).

We measured fusion kinetics using fluorescence dequenching assays. These assays are based in measuring sudden changes in the fluorescence intensity that correspond to fusion events. The dye used to label the viral membrane is at a self-quenching concentration, which means that the fluorescence is not maximal in that state. When fusion occurs, the quenched dye diffuses into the target membrane, its concentration decreases and fluorescence increases (this process is

known as dequenching). This can be monitored by fluorescence microscopy and after data analysis, fusion kinetics curves can be obtained.

In this work, only fusion kinetics curves of spherical viruses could be determined. We conclude that the number of viruses that were present in the filamentous virus sample was too low to measure fusion events using this platform. Therefore, more emphasis needs to be put on reaching a point in which the experimental conditions are good enough for us to detect fusion using viruses that are in a low concentration. Increasing the viral concentration (growing the virus) would be a feasible solution for this. Once achieving these conditions, future experiments may give us information about how different or similar the membrane fusion process is in viruses with totally different shapes. That information will broaden our knowledge of viruses and could be useful for therapeutic purposes and help us beat viral infections.

Introduction

Membrane fusion is a key step in the infectious cycle of enveloped viruses. During this process, the viral and cellular membranes fuse, enabling the release of the viral content into the cell. This mechanism is used by enveloped viruses as an entry mechanism *per se* (e.g., HIV[2]) or to escape from the endosomal compartment prior to fusion with lysosomes to avoid degradation (e.g., DENV[3]). Within the viral families that undergo membrane fusion, there is a wide variety in virion morphology including, in some cases, pleomorphic viral species i.e., viruses that can adopt different morphologies[4]. Different viral shapes described in these families include spherical, filamentous, bacilliform, bullet-shaped or C-shaped particles (Table 1)[4–8].

TABLE 1. Virion morphology of different enveloped viruses that undergo fusion

Species	Acronym	Family	Virion morphology
Influenza A virus	IAV	*Orthomyxoviridae*	Spherical, bacilliform and filamentous*
Respiratory syncytial virus	RSV	*Paramyxoviridae*	Usually spherical*
Ebola virus	EBOV	*Filoviridae*	Bacilliform, filamentous
Human immunodeficiency virus	HIV	*Retroviridae*	Spherical
Severe acute respiratory syndrome coronavirus 2	SARS-CoV-2	*Coronaviridae*	Roughly spherical*
Equine torovirus	EToV	*Coronaviridae*	C-shaped
White bream virus	WBV	*Coronaviridae*	Bacilliform
Dengue virus	DENV	*Flaviviridae*	Spherical
Semliki forest virus	SFV	*Togaviridae*	Spherical
Rabies virus	RABV	*Rhabdoviridae*	Bullet-shaped
Herpes simplex virus	HSV	*Herpesviridae*	Spherical

*pleomorphic

Given the immense heterogeneity in viral geometry among viruses that undergo membrane fusion during their infectious cycle, it is interesting to study if such differences in viral morphology have an impact on fusion kinetics. For this purpose, we chose influenza A virus (IAV) for our study as it is a highly pleomorphic virus presenting both filamentous and spherical particles. Influenza viruses belong to the *Orthomyxoviridae* viral family and are enveloped viruses with segmented negative-sense single stranded RNA (ssRNA(-)) genome composed of eight different linear segments in the case of IAV[9]. Segment 4 codes for haemagglutinin (HA) which is the viral glycoprotein driving receptor binding and fusion between the viral and endosomal membranes (Figure 1A). HA is active in its trimeric form and it is composed of two different subunits (HA1 and HA2) (Fig. 1B). The first subunit mediates binding to sialylated glycans (receptor) while the second subunit is involved in membrane fusion[10]. Trimers present in the viral membrane activate upon endosomal acidification. A conformational change is produced when the protein is exposed to low pH leading to the exposure and insertion of the fusion peptide to the target membrane bringing both membranes together and triggering their fusion[11,12].

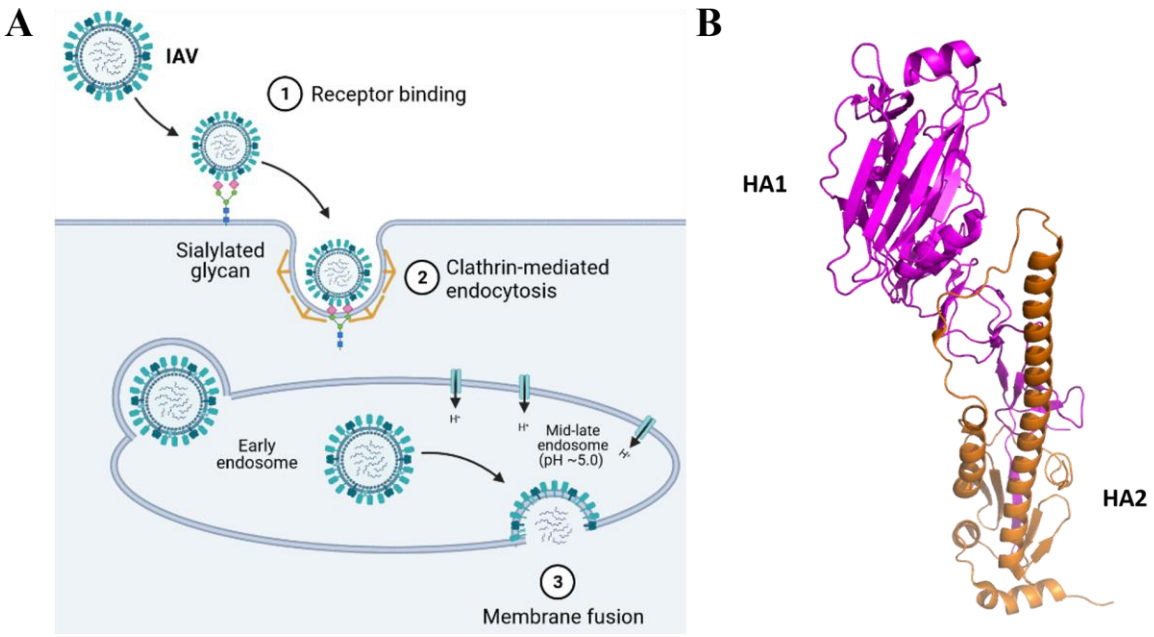

Figure 1. Schematic representation of IAV cell entry and membrane fusion steps of its infectious cycle. Picture adapted from Lee (2010) using BioRender (**A**). Molecular visualization of HA glycoprotein from IAV in its monomeric form (PDB ID: 4UO4). HA1 subunit is represented in magenta and HA2 subunit is represented in orange. Visualization modifications were made using PyMol software (**B**).

Filamentous influenza viral particles are abundant in clinical isolates. However, a morphology change occurs after laboratory passage in eggs or cell cultures[13–15]. Although the role filamentous particles play in the infectious cycle of influenza remains unclear, this observation suggests that there is a selective advantage for the filaments *in vivo* that is lost *in vitro* that probably has to do with its survival in nature[16,17]. Its significance in pathogenesis is still an enigma but some hypotheses have been made. Filaments may facilitate the infection spread *in vivo* by clearing the mucus layer in the upper-respiratory tract via neuraminidase (NA) activity[18,19]. Filamentous virions have more membrane proteins compared to spherical virions

as their length is much longer and, thus, have a more extent lipid membrane containing more functional NA and HA glycoproteins. Clearance of the mucus layer could enable an easier spread of the spherical virions to get into contact with the epithelial cells and infect them. In addition, Vijayakrishnan *et al.*, (2013) described filaments that lacked genome. This leads to another hypothesis that says there could be different sorts of filamentous viral particles with different roles during infection. The filaments lacking genomic segments could serve as a decoy to immune components[20].

In this project, two different viral strains belonging to the H3N2 subtype (X-31 and Udorn strains) were used to study their fusion kinetics. The X-31 strain virions are characterized for having spherical morphology and a size of around 100 nm, whereas the Udorn viral particles form stable filaments variable in length where filaments of few microns long have been reported[17]. In previous studies, it has been shown that the viral matrix proteins M1 and M2, are involved in determining the viral morphology[21–23] and therefore are important for the filament formation. In fact, a point mutation in the M1 protein (Ala41Val) of Udorn viral particles lead to a loss of the filament shape and spherical virions are formed instead[21].

Differences in the entry mechanism for spherical and filamentous influenza virions have been described in previous studies. Influenza viruses with spherical morphology enter the cell primarily via clathrin-mediated endocytosis whereas filamentous particles do by macropinocytosis[24]. The same authors that proved a difference in the entry mechanism for spherical and filamentous influenza, showed that during acidification, fragmentation of the filamentous virions occurred and hypothesized it could enable membrane fusion more efficiently,[24] suggesting there may be a difference in the energetics of the fusion process.

Different groups have measured fusion events between single spherical influenza virions and planar lipid bilayers[25], liposomes[26–28] and endosomes[12] using fluorescence dequenching assays. The principle behind these assays is that membrane fusion can be monitored by measuring how fluorescence intensity changes over time (Fig. 2A). Therefore, they can be used to characterize the fusion process between single viral particles and a target lipid membrane by measuring lipid and/or content mixing. Using these assays, Floyd *et al.*, (2008) showed evidence for kinetic intermediates involved in hemifusion (determined by lipid mixing) following pore formation (determined by content mixing). The authors concluded that multiple active HA trimers were required to initiate membrane fusion[25]. Liu and Boxer (2020) studied the role of cholesterol in the target lipid membrane using fluorescent dye-dequenching assays. Their results suggest that fusion efficiency is enhanced by cholesterol although lipid mixing rate stays unaltered and its kinetics are independent to receptor binding. Thus, the process efficiency is increased by membrane curvature alteration rather than by receptor recruitment[27]. Recently, a new platform for measuring fusion events in a controllable manner within a more physiological environment was developed. Application of fluorescence dequenching assays utilizing virus:endosome conjugates proved that fusion kinetics measured in this platform are comparable to those obtained with synthetic target lipid membranes (e.g. liposomes) except for the fact that a second viral slow-fusing population was characterized[12].

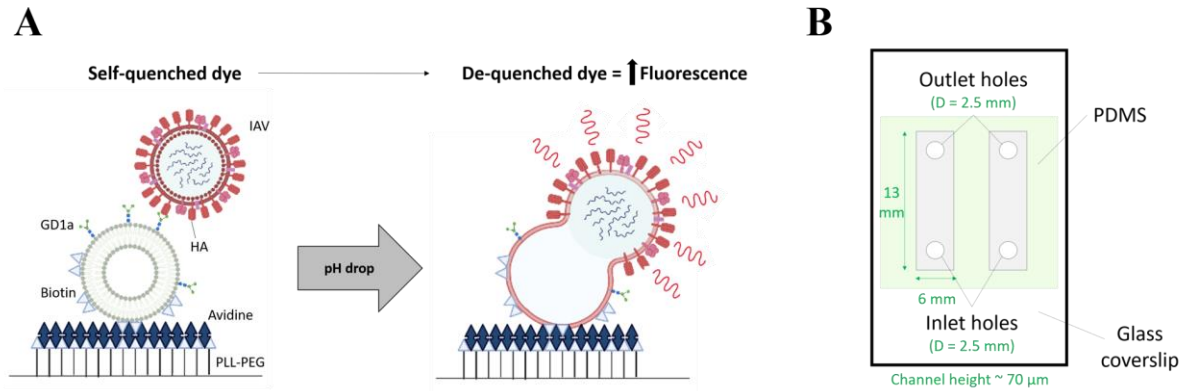

Figure 2. Schematic example representing the experimental design underlying fluorescence dequenching assays used to monitor lipid mixing and study fusion kinetic. The scheme shows the receptor binding of an IAV virion to the liposomal membrane. Following a drop on the pH, fusion is triggered leading to a dilution of the fluorescent dye within the lipid membranes causing the fluorescence intensity to increase due to the dequenching phenomenon. The scheme was made using BioRender (**A**). Scheme of microfluidic flow cells (containing two independent channels) that were built and used in the lipid mixing assays (**B**). Both representations were adapted from Rawle *et al.,* (2016).

As previously mentioned, there are several examples of studies that have used dequenching assays to characterize membrane fusion of spherical virions and whose discoveries have been useful to gain a better understanding of the process. Fluorescence dequenching assays can be used to test, for instance, the efficacy of novel compounds targeting viral fusion. Lipid mixing experiments have been used already for this purpose and have contributed to the finding of potential antivirals inhibiting the fusion process[29–31]. By studying fusion kinetics, we get to deepen in the molecular mechanism of the fusion process and have a better understanding and gain knowledge of every step that is involved with the aim of designing strategies that inhibit the process. However, little is known about the fusion kinetics regarding non-spherical viral particles and whether morphology is an important factor to take into account in the dynamics of membrane fusion. Results from one previous study suggest that the fusion kinetics of filamentous viral particles is different from the spherical virions', that fuse slower in comparison[32]. In this thesis project we aim to address this question by performing fluorescent dye-dequenching assays to monitor hemifusion between spherical or filamentous virions and liposomes.

Aim

The aim of the project was to determine the role viral geometry plays in membrane fusion kinetics. Thus, a pleomorphic virus like influenza was chosen for this purpose as it is a virus that has different morphologies (spherical, filamentous and bacilliform). In addition, this study also had the objective to study cellular lipid environment as a potential factor that could influence fusion of viral and endosomal membranes.

Materials and Methods

Lipids and lipophilic dyes

Palmitoyl-oleoyl-phosphatidylcholine (POPC), Dioleoyl-phosphatidylethanolamine (DOPE), 1,2-dipalmitoyl-*sn*-glycero-3-phosphatidylethanolamine-N-(cap biotin) (DPPE-biotin), Oregon Green-1,2-dihexadecanoyl-*sn*-glycero-3-phosphoethanolamine (OG-DHPE), Texas Red-1,2-dihexadecanoyl-*sn*-glycero-3-phosphoethanolamine (TR-DHPE), octadecyl rhodamine B chloride (R18).

Buffers

HB buffer: 20 mM HEPES, 150 mM NaCl (pH 7.2); Reaction buffer (Rxn buffer): 10 mM NaH_2PO_4, 90 mM sodium citrate, 150 mM NaCl (pH 7.4); Fusion buffer: 10 mM NaH_2PO_4, 90 mM sodium citrate, 150 mM NaCl (pH 5.0); NTE buffer: 100 mM NaCl, 10 mM Tris-Cl, 1 mM EDTA (pH 7.4).

Cell Culture and Infection

Madin-Darby Canine Kidney-2 (MDCK-2) cells were used for viral propagation. This cell line was maintained in Dulbecco's Modified Eagle Medium (DMEM) supplemented with 10% heat-inactivated foetal bovine serum (FBS), 10 mM HEPES and 1% penicillin-streptomycin solution (PS) in an incubator at 37ºC with 5% CO_2. During viral infection, cells were cultured in infection media which was composed of DMEM supplemented with 0.1% FBS, 0.3% bovine serum albumin (BSA), 10 mM HEPES, 1% PS and 1 µg/mL TPCK-treated trypsin.

For viral propagation, sub-confluent cells in T-75 culture flasks were infected at a multiplicity of infection (MOI) of 0.01 and were incubated at 37 ºC with 5% CO_2 for one hour until the viral inoculum was removed and replaced with infection media. The cell culture was monitored for cytopathic effect (CPE) daily using an inverted microscope and the supernatant was harvested when major CPEs were observed.

Viruses

Two different influenza A viral strains belonging to the H3N2 subtype were used in the study. The strain X-31 (A/Aichi/68) was purchased from Charles River Laboratories (Wilmington, MA). The second viral strain used was A/Udorn/72 (Udorn), which was provided kindly by Professor Robert A. Lamb at Northwestern University.

Viral Purification

The Udorn strain used to infect MDCK-2 cells for viral propagation was purified by ultracentrifugation using a SW40-Ti rotor. Harvested media from the infected cell cultures was clarified prior ultracentrifugation by centrifuging at 2600 x g for 10 minutes at 4ºC. Beckman Coulter™ UltraClear centrifuge thin-wall tubes (14 x 95 mm) were used for ultracentrifugation of clarified media through a 30% sucrose cushion in NTE buffer. Ultracentrifugation was performed at 25.000 rpm for 2.5 hours at 4ºC. The pellet was resuspended in 700 µl PBS with

1 mM EDTA, vortexed and allowed to resuspend on ice at 4ºC overnight. The viruses were aliquoted and stored at -80ºC until further use.

Haemagglutination Test

Haemagglutination tests (HA tests) were performed in U-bottom 96-well microtiter plates in 2-fold or 10-fold serial dilutions of the viral stocks from X-31 or Udorn strains. Viral dilutions were done in PBS and no virus was added to the negative controls. To perform the test, 50 µl of a previously prepared red blood cell (RBC) suspension was added to every well and plates were incubated for one hour at room temperature (RT) before the assay results were checked. The RBC suspension was prepared from sheep whole blood cells in Alsever's solution (Håtunalab, Bro, Sweden) in the following manner. To separate the different cell populations and plasma from the blood sample, 4 mL of the whole blood cells were added to 8 mL PBS and centrifuged at 800 x g for 10 minutes at RT. The supernatant (corresponding to plasma) and the buffy layer (where leukocytes and platelets are found), were discarded and the remaining layer containing the RBCs was washed by adding PBS and centrifuging at 800 x g for 10 minutes at RT. This washing step was repeated three times. Finally, the RBC suspension was diluted to make a 1% RBC suspension and it was tested for agglutination at RT for one hour. The 125X dilution was the chosen one to perform the HA tests.

Immunoblotting

Protein gel electrophoresis was performed in denaturing conditions using SDS-PAGE (sodium dodecyl sulphate – polyacrylamide gel electrophoresis) for protein separation. Commercial ready-made gels were used for this (NuPAGE™ 4-12% Bis-Tris Gel; Invitrogen, Carlsbad, CA). After protein separation, the proteins were transferred to a nitrocellulose blotting membrane (Amersham™ Protran™ 0.45 µm NC; GE Healthcare Life Sciences) using Trans-Blot Turbo Transfer System (Bio-Rad Laboratories, Inc., Hercules, CA). When the transfer was completed, the membranes were incubated in 3% skimmed milk blocking solution for one hour prior antibody treatment. Rabbit α-HA (CHA1) was used as a primary antibody (1:1000 dilution) and a goat α-rabbit IgG HRP-conjugated was utilized as the secondary antibody (1:10,000 dilution). After each antibody treatment, the membranes were washed with PBST (PBS with 0.1% Tween-20) while shaking for 15 minutes. The washing steps were repeated three times. Once the membranes were incubated with both antibodies and rinsed, they were treated with 500 µl of a 1:1 mixed solution of luminol and peroxide buffer. These reagents were used as part of the Immun-Star™ HRP Chemisluminiscent Kit (Bio-Rad Laboratories, Inc., Hercules, CA) to trigger the luminescence reaction. Western blots were visualized with Image Lab software using ChemiDoc™ MP Imaging System (Bio-Rad Laboratories, Inc., Hercules, CA). Thermo Scientific™ PageRuler™ Plus Prestained Protein Ladder (10 to 250 kDa) was the reference molecular weight marker used for immunoblotting experiments.

Fluorescent Viral Labelling with Lipophilic Dyes

Influenza A X-31 virions were labelled using TR-DHPE at self-quenching concentration, whilst Udorn virions were labelled with R18 or TR-DHPE in the following manner. The dye solution was prepared by mixing Texas Red (TR) or R18 at 0.75 mg/mL and 1.25 mg/mL respectively in ethanol with HB buffer at a ratio of 1:40. For Udorn viral particles different ratios were tested (1:40, 1:20, 3:40 and 3:20). 36 µl of the dye solution was mixed with 9 µl of viral stock (a

Udorn-labelled batch was also made adding 18 µl of the viral stock instead) and incubated at 600 rpm for two hours at RT. 1.3 mL of HB buffer was added after incubation and tubes were centrifuged at 21,000 x g for 50 minutes at 4°C to pellet the labelled virus. Pellet resuspension was done in 10 µl HB buffer and the tubes were left on ice at 4°C overnight.

Liposome Suspension Preparation

The liposome suspension used in the experiments was prepared by extruding a lipid mixture (66.5% POPC, 20% DOPE, 10% cholesterol, 2% GD1a, 1% DPPE-biotin and 0.5% OG-DHPE) through a nitrocellulose membrane (pore size = 100 nm) an uneven number of times. The extruded liposomes were then stored at 4°C until further use.

Single Virus Lipid Mixing Assay

Single virus lipid mixing assays were performed in polydimethylsiloxane (PDMS) microfluidic flow cells (Fig. 2B) that were built up as previously described[26]. Briefly, PDMS was prepared by mixing silicone elastomer base and curing agent (SYLGARD™ 184 Silicone Elastomer Kit, Ellsworth Adhesives, Germantown, WI) in a 1:10 ratio. The mix was vacuumed for 45 minutes to remove air bubbles. Flow cell molds were filled in with PDMS and incubated at 70°C for two hours until solidified. Once solidified, flow cells were cut (each flow cell contains two channels), inlet and outlet holes were made and the PDMS surface was attached to clean coverslips by 25 seconds glow discharge at 20 mA (PELCO easiGlow™, TED Pella Inc.). Coating of the channels' surface with polylysin (PLL), polyethylene glycol (PEG) and biotin was done by pipetting 5 µl/channel of previously mixed PLL-PEG-biotin and PLL-PEG in a 1:20 ratio and incubating the flow cells at RT for two hours. After incubation, the channels were rinsed with 1 mL deionized water and 1 mL Rxn buffer prior functionalization with avidin. Flow cells were incubated at RT for 40 minutes and then washed with 2 mL Rxn buffer. 10 µl of fluorescently labelled liposome suspension was added into each channel, recirculated several times and let overnight at 4°C. A buffer well was made in the inlet hole by cutting the end of a 1000 µL plastic pipette tip and gluing it with five-minute epoxy. The channels were washed again with 2 mL Rxn buffer prior addition of the labelled virions (5 µl/channel), which were recirculated in the channel to favour receptor binding. Labelled X-31 viral particles were diluted five times in Rxn buffer before they were added to the channels. To measure fusion events, each channel was connected to a suction system that enabled buffer exchange. Fusion was triggered by infusing fusion buffer (pH 5.0) and single virus-liposome lipid mixing was monitored by fluorescence microscopy.

Antibody Treatment in Flow Cells

For the antibody treatment, flow cells were prepared as mentioned before, except the liposome suspension used was not fluorescently labelled (Fig. 3). For the primary antibody treatment, 10 µl of a 50X diluted solution of mouse α-H3 HA (HC3) in Rxn buffer was infused in each channel and flow cells were incubated at RT for two hours. Subsequently, 2 mL Rxn buffer was used to wash the channels and the secondary antibody was added. 5 µl of a 1000X diluted solution of α-mouse IgG FITC in PBS was used. Incubation of the flow cells was done at RT for 1.5 hours and flow cells were rinsed with 2 mL Rxn buffer.

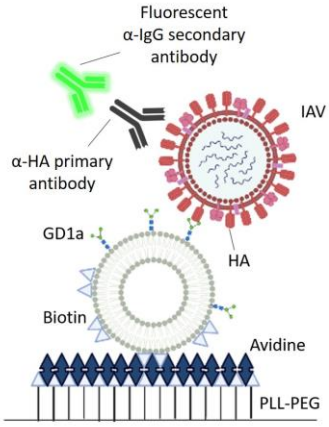

Figure 3. Scheme showing how labelled viral particles bound to non-fluorescent liposomes in a flow cell were labelled with a primary antibody (anti-HA) and targeted with a fluorescent secondary antibody. The scheme was made with BioRender and adapted from Rawle *et al.*, (2016).

Microscopy

A Zeiss Axio Observer inverted microscope was used to take all epifluorescence images and videos using a 100X oil immersion objective (NA = 1,3 (Zeiss)) connected to an Andor Zyla sCMOS camera (Andor Technologies, Belfast, UK) that was used to take pictures using 16-bit image settings and captured with Micromanager software.

Results

Single Virus-Liposome Lipid Mixing Assays with Spherical Virions

Hemifusion between the viral membrane of X-31 virions and the liposomal membrane was measured by monitoring lipid mixing in microfluidic devices. Viral particles were labelled with a lipophilic dye at a self-quenching concentration so that when fusion is triggered by lowering the pH, the fluorescent dye dilutes into the target lipid membrane and fluorescence increases consequently. By measuring the fluorescent signal during the process, we are able to determine lipid mixing corresponding to membrane hemifusion and characterize the kinetics underlying membrane fusion events. To do this, fluorescent liposomes were immobilized in microfluidic flow cells via biotin-avidin interactions and labelled viruses were added subsequently. The HA viral glycoprotein recognises GD1a molecules present in the liposomes' membrane and will bind to these. Particles will not fuse until fusion is triggered by a pH drop. This was accomplished by performing a buffer exchange (from pH 7.4 to pH 5.0) within the flow cells. Waiting times, i.e., the lapse between the pH drop and a sudden increase in fluorescence which reports the lipid mixing, were plotted as a cumulative distribution function (CDF) (Fig. 4) after analyzing the recorded videos. Most fusion events occur within 50 seconds after the pH drop. A minor part of the events that were observed took place at later times. The efficiency percentage of the process was ~17%, which was calculated as the percentage of viral particles that fused relative to the total number of viral particles detected in the field.

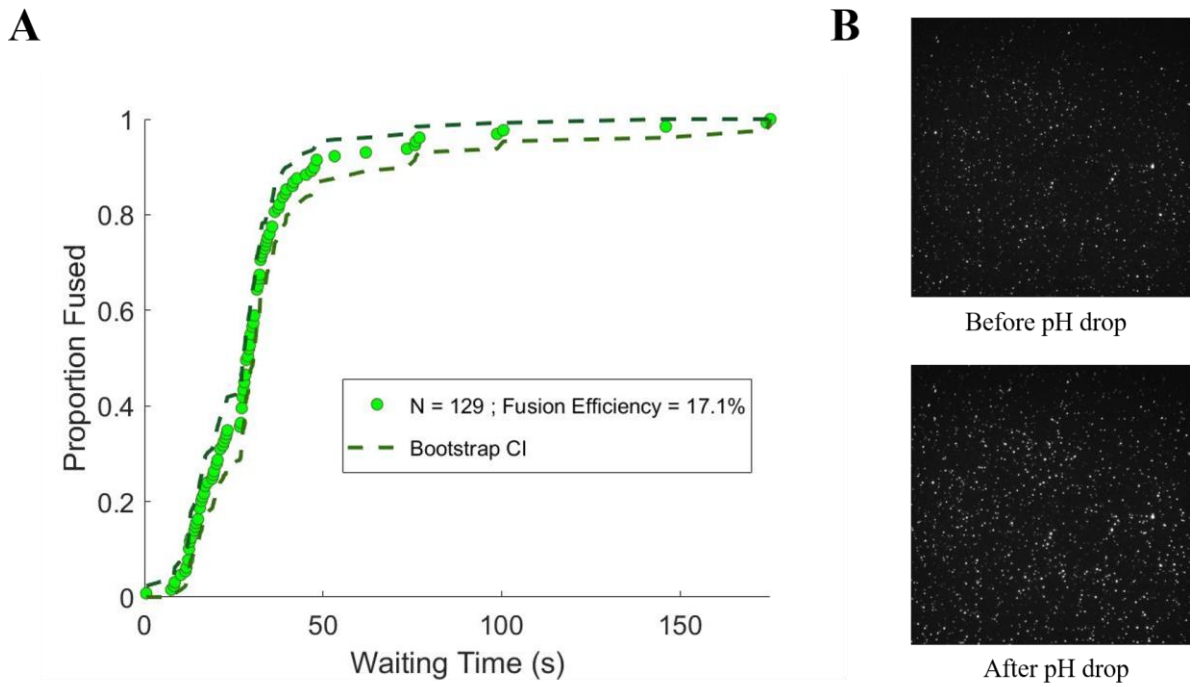

Figure 4. Cumulative Distribution Functions (CDFs) of lipid mixing waiting times distributions for single-virus fusion events, along with bootstrap resampling error estimates (95% confidence intervals (CI)) (**A**). Snapshots of the X-31 viral particles labelled with Texas Red at a virus:dye ratio of 1:5 taken before and after the buffer exchange that clearly manifest the increase in fluorescence as a consequence of fusion (**B**).

Single Virus-Liposome Lipid Mixing Assays with Filamentous Virions

The same strategy was followed to measure fusion events with filamentous virions, using in this case, the Udorn strain. When using the same viral labelling conditions as used for the X-31 virions (dye concentration of 10 µM), no fusion events could be observed when performing the lipid mixing assays. Thus, some modifications were made regarding the viral labelling step in order to accomplish a self-quenching concentration of the dye used. Despite different dye concentrations (20 µM, 30 µM and 60 µM) being tested, none of them yielded fusion when performing the fluorescence dequenching assays using TR. Thus, R18 was used as an alternative fluorescent dye to TR and several dye concentrations (33 µM, and 95 µM) were tested again resulting in no observed fusion events for any of them. The next step that was performed was to increase the amount of virus used for labelling. The previous trials along with the viral labelling of the X-31 strain were made using a virus:dye ratio of 1:5. We decided to double the amount of virus used maintaining constant the quantity of dye solution, meaning that a ratio of 1:3 was tested instead. This time, a single fusion event could be measured when monitoring lipid mixing in one of the flow cells using R18 at a concentration of 41 µM. The fusion event was clearly seen by eye when watching the recording (Fig. 5A) and it was later confirmed by video software analysis. Fluorescence intensity of each particle is measured as a function of time during the analysis. Hence, monitoring the sudden changes on the intensity signal enables the determination of the timepoints when a fusion event occurred (Fig. 5B), in this case approximately 13 s after the pH drop. The software produces individual plots of fluorescence intensity against time for each particle and classifies them into particles that fused, particles that did not fuse and particles whose increase in fluorescence intensity happened too slow for it to be considered a fusion event. To check how well the coating of the flow cells and

the liposome immobilization was, snapshots of the fluorescently labelled liposomes were taken prior fusion triggering in all of the experiments performed. As shown in Figure 5C with two snapshot examples, the flow cells were nicely coated with liposomes in all experiments that were made, both with X-31 and Udorn virions. Barely any spaces were found throughout the entire channel indicating a successful coating of the microfluidic flow cells.

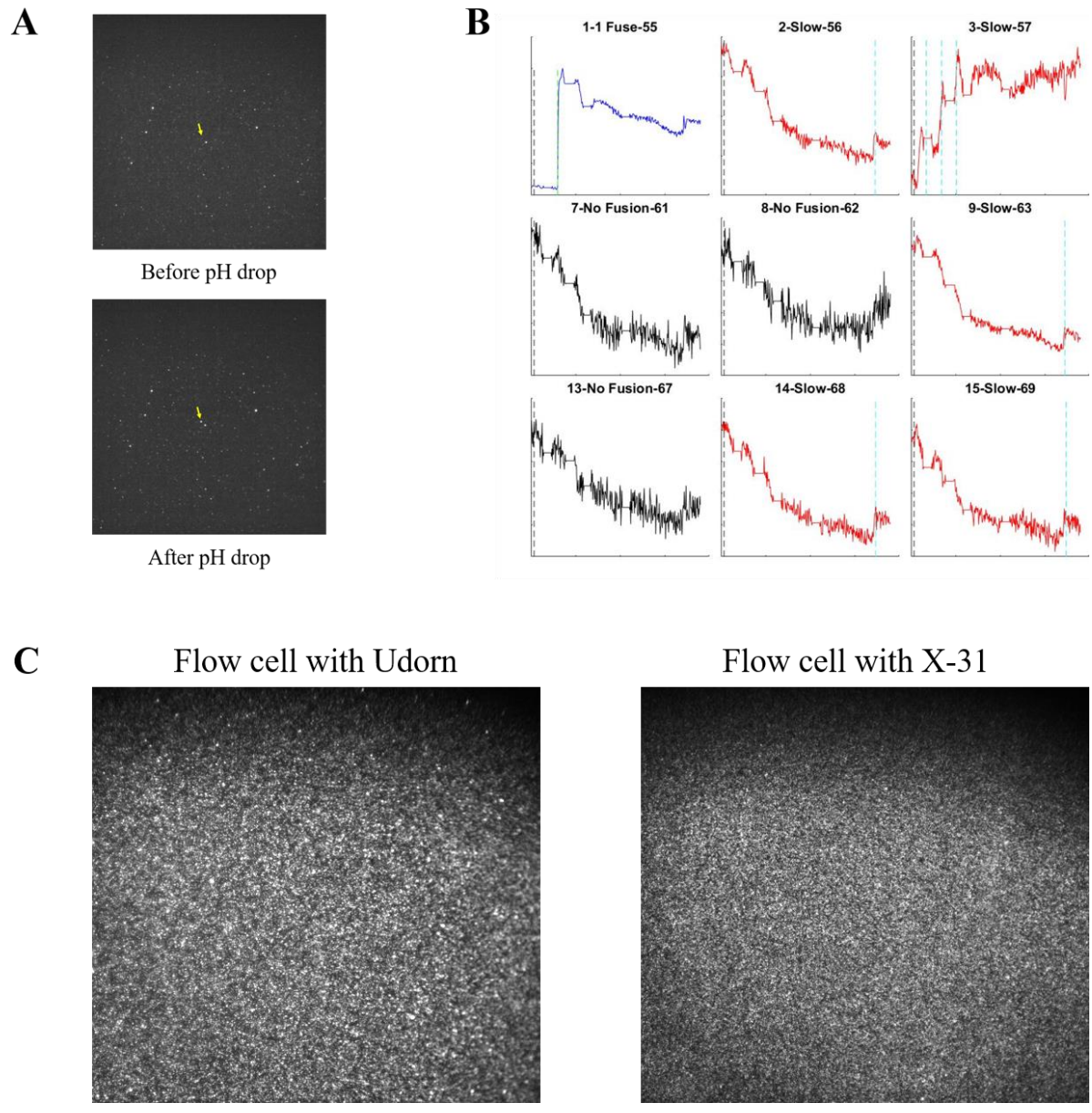

Figure 5. Snapshots of the Udorn viral particles labelled with R18 at a virus:dye ratio of 1:3 taken before and after the pH drop. The yellow arrow is pointing to the single particle that yielded a fusion event under these experimental conditions (**A**). Plots made during video analysis showing fluorescence intensity (Y-axis) against time (X-axis). The pattern corresponding to particles that fused (blue) is evidently different to the rest, which represent no fusion events (black) or particles with a slow jump in their fluorescence (red) which are not considered as fusion events (**B**). Image examples showing fluorescently labelled liposomes immobilized in the flow cells. The one to the left corresponds to a flow cell that was used to measure fusion events with Udorn, whereas the flow cell on the right picture was used with X-31 (**C**).

Antibody Labelling of Viral Particles in Flow Cells

Due to the lack of fusion events observed with filamentous viral particles, we decided to set up an experiment in which we could detect how many of the dye-positive (having used either TR or R18 to label the virus) particles were actual viruses. This was done by antibody labelling using a primary anti-HA antibody that recognises and binds to the viral hemagglutinin and a fluorescent secondary antibody. Controls without addition of virus or primary antibody were included (see Appendix A). Results show that there is a higher level of colocalization for the X-31 strain compared to the Udorn (Fig. 6), i.e., a great percentage of the red fluorescent particles that are observed are indeed viral particles in the case of X-31 strain.

Udorn labelled with R18 X-31 labelled with TR

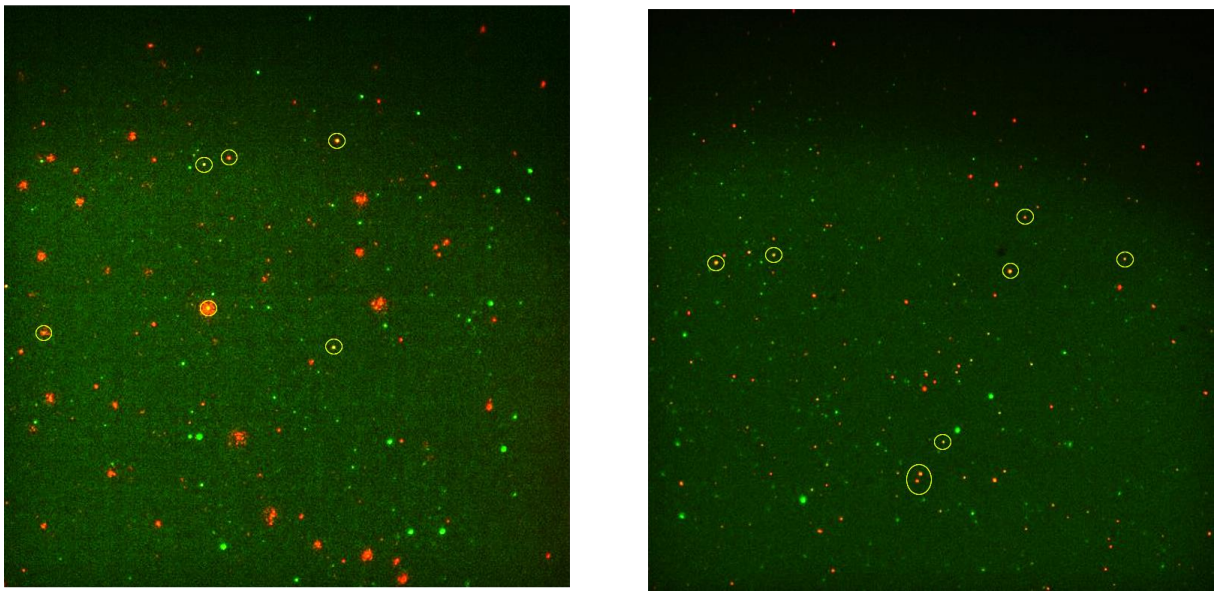

Figure 6. The left image shows colocalization (orange) between R18-positive Udorn particles (red) and the antibody signal (green), whereas the picture to the right shows colocalization with TR-positive X-31 particles instead. The yellow circles indicate some colocalization points (not all of them are indicated in the X-31 picture).

Haemagglutination Test

An HA test using both viral stocks was performed to check and compare the HA titres of both stocks. This test is based on the absence of agglutination of RBCs that is observed in presence of HA giving a rough idea about the viral concentration of both Udorn and X-31 viral stocks. To do this, 2-fold serial dilutions of the viral stocks in PBS were performed (Fig. 7A) and RBCs were added to each well at the same concentration. In addition, negative controls were included in which no virus was added. The X-31 strain showed agglutination for all the dilutions tested and due to this, the assay was repeated with the X-31 strain in a 10-fold serial dilution of the virus (Fig. 7B). Results from this assay show that the X-31 viral stock (HA titre of 10^6 HAU) is significantly more concentrated than the Udorn stock (HA titre of 32 HAU), i.e., there are more viral particles present in the X-31 stock compared to Udorn.

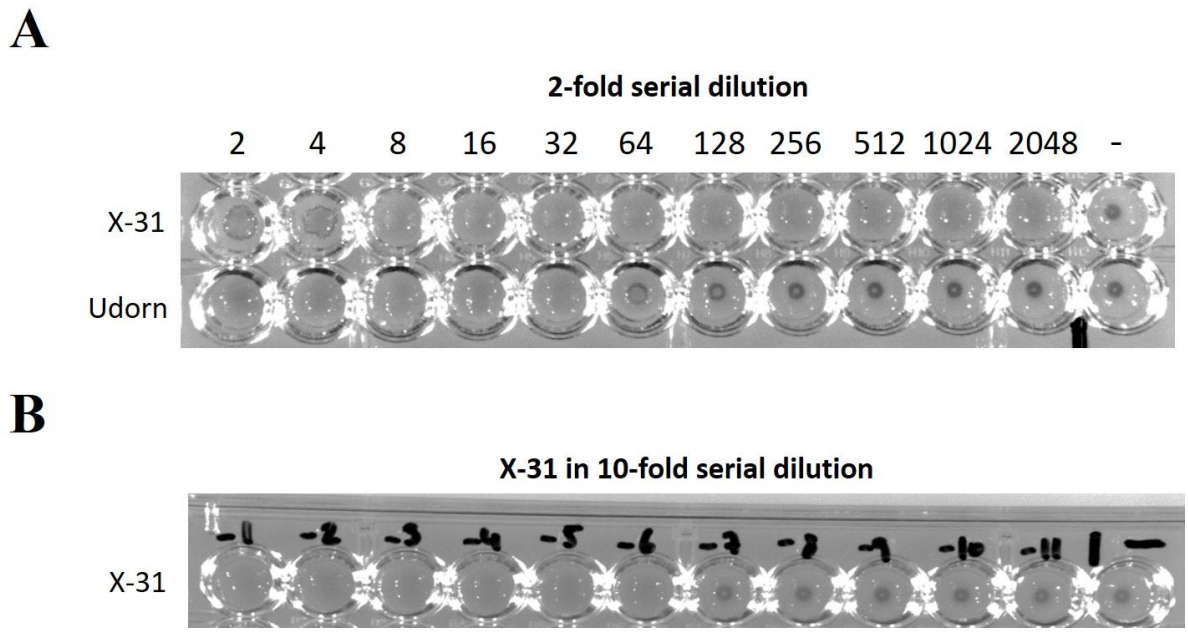

Figure 7. HA test results doing a 2-fold serial dilution of viral stocks from X-31 and Udorn strains (**A**). HA test results of the X-31 viral stock doing a 10-fold serial dilution (**B**). The "-" sign indicates the negative control in which no virus was added.

Viral Propagation of Udorn Virus in MDCK-2 Cells

A viral amplification of the Udorn strain in cell culture was performed in order to produce a viral batch with a higher titre. During cell infection, a CPE difference was observed between the two infected T-75 flasks. Although CPE signs were not that evident in either of the flasks, one of them clearly showed more signs (referred to as "+") than the other one (referred to as "–"). Due to the lack of observable CPE signs or cell detachment after 2 – 3 days post-infection (dpi), the flasks were incubated for longer time and eventually the media was harvested at 7 dpi, when the viral purification was made. Purified samples from both "+" and "–" flasks along with the viral stocks from Udorn and X-31 strains (which served as a control) were tested for viral presence via immunoblotting. Results from the western blot show the presence of bands corresponding to HA in both viral controls and for the "+" purified sample (Fig. 8A). Furthermore, the HA titre of the "+" sample was determined by an HA assay. As shown in Figure 8B, the HA titre for this sample was of 16 HAU, as that is the last well where absence of agglutination can be observed.

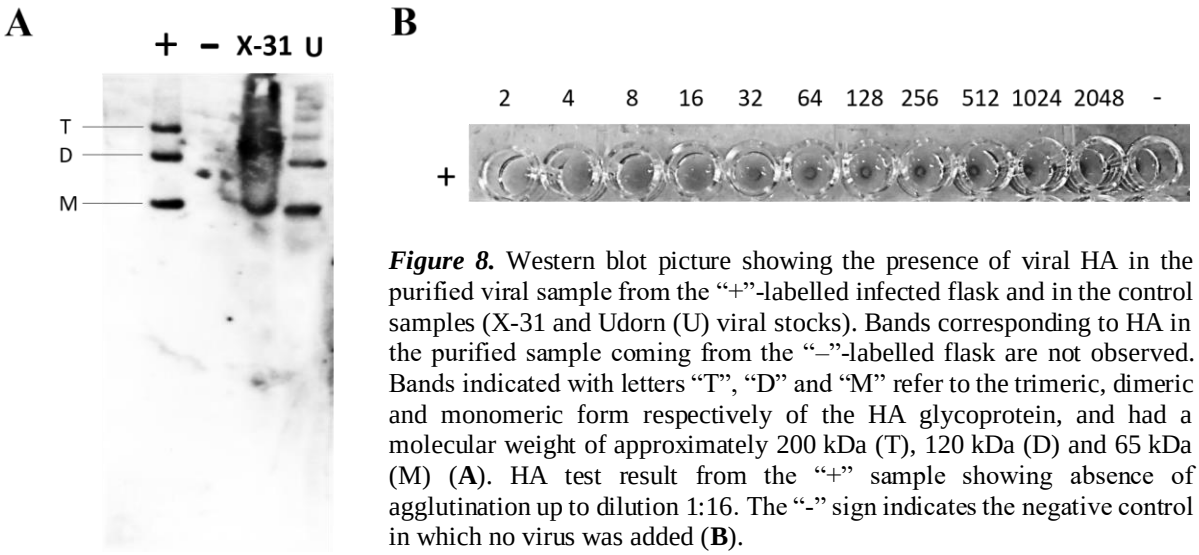

Figure 8. Western blot picture showing the presence of viral HA in the purified viral sample from the "+"-labelled infected flask and in the control samples (X-31 and Udorn (U) viral stocks). Bands corresponding to HA in the purified sample coming from the "–"-labelled flask are not observed. Bands indicated with letters "T", "D" and "M" refer to the trimeric, dimeric and monomeric form respectively of the HA glycoprotein, and had a molecular weight of approximately 200 kDa (T), 120 kDa (D) and 65 kDa (M) (**A**). HA test result from the "+" sample showing absence of agglutination up to dilution 1:16. The "-" sign indicates the negative control in which no virus was added (**B**).

Discussion

As results show, measurement of fusion events between liposomes and spherical virions were performed successfully. However, comparison of the fusion kinetics of filamentous and spherical virions could not be made as we did not manage to measure fusion with the Udorn strain. There are diverse reasons for this, and it is most likely that a combination of these factors explain why we were not able to detect any fusion events.

Firstly, as the performed HA tests suggest, there is a big difference in the viral concentration of both stocks, which in practical terms means that the initial number of virions used for labelling was very different. According to the results from the HA test the X-31 viral stock contains substantially more particles than the Udorn stock. This could be a factor to take into consideration and could be one reason that would explain why no fusion events could be accounted. It is very likely that if the viral stock that was used for viral labelling was in such low concentration, there were not enough fusogenic labelled viral particles to enable the lipid mixing monitoring in the microfluidic flow cells. In addition, one has to consider the further loss of viral particles that inevitably occurs during the labelling steps. Secondly, it is possible that a self-quenching concentration of the dye used to label the filamentous viruses was not properly achieved. Therefore, despite detecting fluorescence in the microscope, if the dye is not quenched, we would not be able to detect and measure potential fusion events happening in the channels as the fluorescence intensity would remain invariable upon the pH drop induced by the buffer exchange. Different labelling conditions were assessed to try to find an optimal condition in which the dye would be self-quenched. The first trials with TR (the same dye that was used with X-31 virions) were unsuccessful and no fusion events could be detected. An alternative lipophilic fluorescent dye, R18, was tested. This dye has a single hydrophobic tail, which favours its partition into the lipidic membrane. Despite the various conditions that were tried, using different dye concentrations (to try to improve and reach a self-quenching concentration) and virus:dye ratios (to increase the amount of virus in the labelling batch), only one single fusion event could be measured when the Udorn particles were labelled with R18 at a virus:dye ratio of 1:3, resulting in a final dye concentration of 41 µM.

We hypothesize that in that condition, a self-quenching concentration of R18 was achieved but that there were not enough labelled particles to be able to monitor lipid mixing and obtain information regarding fusion kinetics. Thus, in order to use this system to measure fusion events, a higher concentration of virus is needed. This could be achieved, for instance, by prior amplification of the virus in tissue cultures so that higher viral titres are reached. Moreover, the results from the antibody labelling of the viruses in the flow cells support this fact. Not enough labelled viruses were present as we could observe very little colocalization of the fluorescent signals coming from the lipophilic dye used to label the virus (red) and the antibody (green) in the flow cell containing Udorn. This did not happen with X-31 viral particles, where the colocalization was much higher. However, it is worth pointing to the presence of an important number of green dots, which would correspond merely to non-labelled viruses, in both flow cells. This can give us an idea of how many viral particles remain unlabelled after the membrane labelling.

It can be concluded that an optimization of the viral labelling is required for low titre virus samples as in the case of Udorn strain. A higher yield in the labelling procedure minimizing the unlabeled viral particles may compensate for their low number. Additionally, successful viral propagation of low titre strains would also be convenient before starting with lipid mixing experiments. Although this was tried in this study, the HA viral titre yield was not higher compared to the viral stock. This could be due to an inadequate infection procedure of the cell cultures since in the "–" flask, cells were clearly not infected and many factors could be involved in this negative result (inappropriate MOI used, too confluent cells, pipetting errors, etc.).

As an optimal labelling condition of the filamentous virus was not accomplished, experiments to determine the impact of cellular lipid environment were not performed although it was part of the aim of this project. For future steps, once having achieved an acceptable viral labelling appropriate for measuring lipid mixing using Udorn, it would be interesting to measure fusion kinetics in virus:endosome conjugates rather than with liposomes. In that case we would be measuring fusion events in a more physiological environment and within a context that approximates much better to reality. Much focus has been put in studying the properties of viral proteins responsible for triggering fusion and serving as catalysts in the process, such as the HA of IAV[32–34]. However, the cellular lipid environment may also have an important impact on fusion kinetics, and this remains to be addressed. These experiments in which endosomes containing viruses are isolated and immobilized in a microfluidic flow cell and lipid mixing is monitored, could give new information about how important any cellular lipid component would be during membrane fusion. This has been previously done using spherical viral particles[12] but not with a filamentous virus, such as the Udorn strain from IAV.

Acknowledgements

I would like to thank my supervisor and co-supervisor for everything they have taught me on the way to making this thesis project and to all other researchers from the department for the helpful discussions. Last but not least, to my family and friends for all their support and love. To all of them, thank you.

References

1. Prioritizing diseases for research and development in emergency contexts. https://www.who.int/activities/prioritizing-diseases-for-research-and-development-in-emergency-contexts.
2. HIV Replication Cycle | NIH: National Institute of Allergy and Infectious Diseases. https://www.niaid.nih.gov/diseases-conditions/hiv-replication-cycle.
3. Schaar, H. M. van der *et al.* Dissecting the Cell Entry Pathway of Dengue Virus by Single-Particle Tracking in Living Cells. *PLOS Pathogens* **4**, e1000244 (2008).
4. Gelderblom, H. R. Structure and Classification of Viruses. in *Medical Microbiology* (ed. Baron, S.) (University of Texas Medical Branch at Galveston, 1996).
5. Harrison, M. S., Sakaguchi, T. & Schmitt, A. P. Paramyxovirus Assembly and Budding: Building Particles that Transmit Infections. *Int J Biochem Cell Biol* **42**, 1416–1429 (2010).
6. Family - Filoviridae. in *Virus Taxonomy* (eds. King, A. M. Q., Adams, M. J., Carstens, E. B. & Lefkowitz, E. J.) 665–671 (Elsevier, 2012). doi:10.1016/B978-0-12-384684-6.00055-0.
7. Family - Coronaviridae. in *Virus Taxonomy* (eds. King, A. M. Q., Adams, M. J., Carstens, E. B. & Lefkowitz, E. J.) 806–828 (Elsevier, 2012). doi:10.1016/B978-0-12-384684-6.00068-9.
8. Family - Retroviridae. in *Virus Taxonomy* (eds. King, A. M. Q., Adams, M. J., Carstens, E. B. & Lefkowitz, E. J.) 477–495 (Elsevier, 2012). doi:10.1016/B978-0-12-384684-6.00044-6.
9. S. Jane Flint, Lynn W. Enquist, Vincent R. Racaniello, Glenn F. Rall, Anna Marie Skalka. *Principles of Virology*. vol. 2 (ASM Press, 2015).
10. Skehel, J. J. & Wiley, D. C. Receptor Binding and Membrane Fusion in Virus Entry: The Influenza Hemagglutinin. *Annu. Rev. Biochem.* **69**, 531–569 (2000).

11. Lee, K. K. Architecture of a nascent viral fusion pore. *The EMBO Journal* **29**, 1299–1311 (2010).

12. Haldar, S., Okamoto, K., Dunning, R. A. & Kasson, P. M. Precise Triggering and Chemical Control of Single-Virus Fusion within Endosomes. *Journal of Virology* **95**, (2020).

13. Dadonaite, B., Vijayakrishnan, S., Fodor, E., Bhella, D. & Hutchinson, E. C. Filamentous influenza viruses. *Journal of General Virology*, **97**, 1755–1764 (2016).

14. Chu, C. M., Dawson, I. M. & Elford, W. J. FILAMENTOUS FORMS ASSOCIATED WITH NEWLY ISOLATED INFLUENZA VIRUS. *The Lancet* **253**, 602–603 (1949).

15. Choppin, P. W., Murphy, J. S. & Tamm, I. STUDIES OF TWO KINDS OF VIRUS PARTICLES WHICH COMPRISE INFLUENZA A2 VIRUS STRAINS. *J Exp Med* **112**, 945–952 (1960).

16. Kordyukova, L. V. *et al.* Filamentous versus Spherical Morphology: A Case Study of the Recombinant A/WSN/33 (H1N1) Virus. *Microscopy and Microanalysis* **26**, 297–309 (2020).

17. Li, T. *et al.* Phenotypic heterogeneity in particle size is a viral mechanism of persistence. *bioRxiv* 843177 (2020) doi:10.1101/843177.

18. Seladi-Schulman, J., Campbell, P. J., Suppiah, S., Steel, J. & Lowen, A. C. Filament-producing mutants of influenza A/Puerto Rico/8/1934 (H1N1) virus have higher neuraminidase activities than the spherical wild-type. *PLoS One* **9**, e112462 (2014).

19. Cohen, M. *et al.* Influenza A penetrates host mucus by cleaving sialic acids with neuraminidase. *Virol J* **10**, 321 (2013).

20. Vijayakrishnan, S. *et al.* Cryotomography of Budding Influenza A Virus Reveals Filaments with Diverse Morphologies that Mostly Do Not Bear a Genome at Their Distal End. *PLOS Pathogens* **9**, e1003413 (2013).

21. Roberts, P. C., Lamb, R. A. & Compans, R. W. The M1 and M2 proteins of influenza A virus are important determinants in filamentous particle formation. *Virology* **240**, 127–137 (1998).

22. Kolpe, A. *et al.* Super-resolution microscopy reveals significant impact of M2e-specific monoclonal antibodies on influenza A virus filament formation at the host cell surface. *Scientific Reports* **9**, 4450 (2019).

23. Elleman, C. J. & Barclay, W. S. The M1 matrix protein controls the filamentous phenotype of influenza A virus. *Virology* **321**, 144–153 (2004).

24. Rossman, J. S., Leser, G. P. & Lamb, R. A. Filamentous Influenza Virus Enters Cells via Macropinocytosis. *J Virol* **86**, 10950–10960 (2012).

25. Floyd, D. L., Ragains, J. R., Skehel, J. J., Harrison, S. C. & Oijen, A. M. van. Single-particle kinetics of influenza virus membrane fusion. *PNAS* **105**, 15382–15387 (2008).

26. Rawle, R. J., Boxer, S. G. & Kasson, P. M. Disentangling Viral Membrane Fusion from Receptor Binding Using Synthetic DNA-Lipid Conjugates. *Biophys J* **111**, 123–131 (2016).

27. Liu, K. N. & Boxer, S. G. Target Membrane Cholesterol Modulates Single Influenza Virus Membrane Fusion Efficiency but Not Rate. *Biophys J* **118**, 2426–2433 (2020).

28. Gui, L. & Lee, K. K. Influenza Virus-Liposome Fusion Studies using Fluoresence Dequenching and Cryo-Electron Tomography. *Methods Mol Biol* **1836**, 261–279 (2018).

29. Huang, Kelly, Incognito, Len, Chen, Xing, Ulbrandt, Nancy D., & Wu, Herren. Respiratory Syncytial Virus-Neutralizing Monoclonal Antibodies Motavizumab and Palivizumab Inhibit Fusion. *J Virol* **84**, 8132–8140 (2010).

30. Ohki, S., Liu, J.-Z., Schaller, J. & Welliver, R. C. The compound DATEM inhibits respiratory syncytial virus fusion activity with epithelial cells. *Antiviral Research* **58**, 115–124 (2003).

31. Rowse, M. *et al*. Characterization of Potent Fusion Inhibitors of Influenza Virus. *PLOS ONE* **10**, e0122536 (2015).

32. Ivanovic, T., Choi, J. L., Whelan, S. P., van Oijen, A. M. & Harrison, S. C. Influenza-virus membrane fusion by cooperative fold-back of stochastically induced hemagglutinin intermediates. *eLife* **2**, e00333 (2013).

33. White, J. M., Delos, S. E., Brecher, M. & Schornberg, K. Structures and Mechanisms of Viral Membrane Fusion Proteins. *Crit Rev Biochem Mol Biol* **43**, 189–219 (2008).

34. Wilson, I. A., Skehel, J. J. & Wiley, D. C. Structure of the haemagglutinin membrane glycoprotein of influenza virus at 3 Å resolution. *Nature* **289**, 366–373 (1981).

Appendix A

Appendix A contains supplementary figures that support or complement the figures shown in the results section.

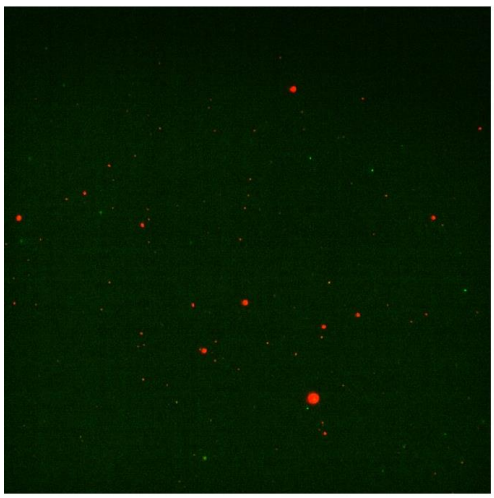

Control with no primary antibody

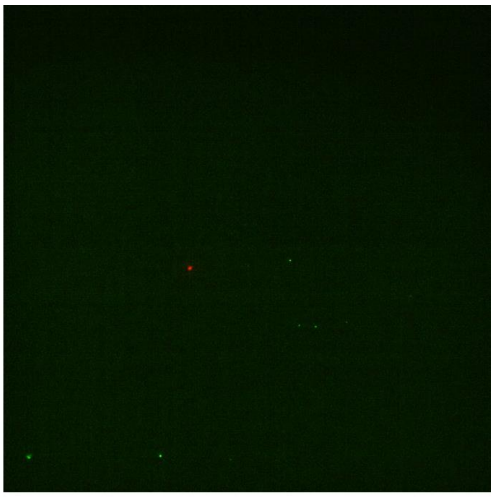

Control with no virus

Figure 9. These images show the control channels that were performed for the antibody viral labelling in the microfluidic flow cells and inform about the non-specific binding of the antibodies. The picture to the left shows the control where no primary antibody was added (no colocalization is observed), while no virus was added to the flow cell of the right picture.